

Banner appropriate to article type will appear here in typeset article

Friction and heat transfer in forced air convection with variable physical properties

Davide Modesti¹† and Sergio Pirozzoli²

¹Faculty of Aerospace Engineering, Delft University of Technology, Kluyverweg 2, 2629 HS Delft, The Netherlands

²Dipartimento di Ingegneria Meccanica e Aerospaziale, Sapienza Università di Roma, via Eudossiana 18, 00184 Roma, Italia

(Received xx; revised xx; accepted xx)

We establish a theoretical framework for predicting friction and heat transfer coefficients in variable-properties forced air convection. Drawing from concepts in high-speed wall turbulence, which also involves significant temperature, viscosity, and density variations, we utilize the mean momentum balance and mean thermal balance equations to develop integral transformations that account for the impact of variable fluid properties. These transformations are then applied inversely to predict the friction and heat transfer coefficients, leveraging the universality of passive scalars transport theory. Our proposed approach is validated using a comprehensive dataset from direct numerical simulations, covering both heating and cooling conditions up to a friction Reynolds number of approximately $Re_\tau \approx 3200$. The predicted friction and heat transfer coefficients closely match DNS data with an accuracy margin of 1-2%, representing a significant improvement over the current state of the art.

Key words: Forced convection; Heat transfer; Variable fluid properties; Wall turbulence

1. Introduction

Heat transfer by turbulent forced convection occurs when a cold fluid flows over a hot wall, or vice versa. Forced thermal convection has countless applications in engineering, and it is the fundamental principle upon which heat exchangers are designed and built (Incropera *et al.* 1996; Kakac *et al.* 2002). Heat exchangers are a key component in any energy conversion system, for instance, the radiators in our homes, heat pumps, fuel cells, nuclear plants, and solar receivers. In aerospace engineering, two notable applications are aircraft and rocket engines, where components are subjected to extreme heat loads and internal cooling is necessary to guarantee the material integrity.

Most studies on forced thermal convection regard the temperature field as a passive scalar, neglecting its feedback effect on the velocity field through the variation of the transport properties of the fluid. Notable experimental and numerical studies relying on the constant-property assumption are the ones by Sparrow *et al.* (1966); Xia *et al.* (2022); Alcántara-

† Email address for correspondence: d.modesti@tudelft.nl

Ávila *et al.* (2021); Abe & Antonia (2017), together with the more recent direct numerical simulation (DNS) studies performed by our group (Pirozzoli *et al.* 2016; Pirozzoli & Modesti 2023).

The constant-property assumption is valid if temperature variations are on the order of a few percent because the thermodynamic variables and fluid properties can be assumed to be constant (Cebeci 1973). However, most engineering applications feature large temperature differences. For instance, in aircraft engines, the air passing through the cooling channels of turbine blades has a mean temperature $T_m \approx 400\text{K}$, whereas the wall temperature reaches $T_w \approx 800\text{K}$, hence their ratio is well beyond the range of validity of the constant-property assumption. This range of temperature variations is common in engineering applications, however the constant-property assumption is used in most academic research and exploited in the engineering practice.

Preliminary design of cooling/heating ducts is based mainly on predictive formulas for the Nusselt number and the pressure drop, which are used for sizing the cooling passages. Among the most classical engineering formulas, we recall those by Dittus–Boelter (Dittus & Boelter 1933) and Gnielinski (Gnielinski 1976) for the Nusselt number, and Prandtl’s friction formula for the pressure drop (Nikuradse 1933). Although their use is widespread in engineering design, these formulas are based on the constant-property assumption and do not directly account for the effect of variable fluid properties, which is usually included using empirical corrections (Yeh & Stepka 1984; Sleicher & Rouse 1975).

The most popular empirical corrections for heat transfer prediction in water are those by Dittus & Boelter (1985) and Sieder & Tate (1936), which account for the fluid viscosity variations through an empirical corrective factor $(\mu_b/\mu_w)^n$ applied to the Nusselt number resulting from formulas obtained for the constant-property case, where μ_m and μ_w are the viscosities of the fluid evaluated at the mean and wall temperatures, respectively. Also for gases, many empirical predictive formulas for the Nusselt number are available, and they have been reviewed extensively by Petukhov (1970); Yeh & Stepka (1984). However, they all have a similar structure to those used for water, relying on a correction factor based on the mean-to-wall temperature ratio $(T_m/T_w)^n$, with exponent n depending on the type of gas and on the cooling/heating ratio. Similar corrections are also used to estimate the friction factor and they suggest drag reduction in the case of wall heating, both for liquids (Sieder & Tate 1936) and gases (Yeh & Stepka 1984), compared to the adiabatic case. However, these corrections are fluid-dependent, are available only for a limited number of fluids, and their accuracy is often questionable.

More recently, some authors have studied forced thermal convection in fluids with variable properties using DNS. Zonta *et al.* (2012) performed DNS of water flow in a plane channel with a heated and a cold wall and found a reduction of the Reynolds shear stress and of the friction coefficient at the heated wall, despite the lower viscosity which increases the local Reynolds number. Lee *et al.* (2013) performed DNS of turbulent boundary layers with temperature-dependent viscosity representative of water and investigated the effect of wall heating on the friction and heat transfer coefficients. They reported a 26% drag reduction for water with a freestream-to-wall temperature ratio of 0.77, at a freestream temperature of about 300K, and the drag reduction mechanism was attributed to a reduction of the wall-shear stress, in agreement with the findings of Zonta *et al.* (2012). Lee *et al.* (2014) used the same DNS dataset to assess heat transfer modifications due to variable viscosity effects and proposed a correction to the classical Kader’s fitting for the mean temperature profile (Kader 1981). Patel *et al.* (2016, 2017) studied the effects of variable density and viscosity in liquid-like and gas-like fluids using DNS. They utilized compressibility transformations, originally developed for high-speed boundary layers (Modesti & Pirozzoli 2016; Trettel & Larsson 2016), to map velocity and temperature profiles to the constant-properties case, reporting

good agreement with the constant properties profiles. Kaller *et al.* (2019) conducted a wall-resolved large-eddy simulation of flow in a duct with one heated side, filled with water, and observed reduced friction near the heated wall, which was also accompanied by weakened secondary flows. The effect of density variations is also important in the context of mixed convection, although the common practice is to rely on the Boussinesq approximation (Pinelli *et al.* 2010; Pirozzoli *et al.* 2017; Yerragolam *et al.* 2024), whereas studies that account for non-Oberbeck–Boussinesq effect are more limited (Zonta 2013).

Although studies focusing on the effect of density and viscosity variations in forced thermal convection are available, predictive formulas for the heat transfer and friction coefficients are invariably based on empirical fitting of experimental data, and the few numerical studies available did not discuss in detail the prediction of these coefficients. In this study, we aim to develop a more solid theoretical framework to estimate the mean friction drag and heat transfer in the presence of variation of the transport properties, focusing on the case of air as working fluid. For that purpose, we use DNS data of plane turbulent channel flow at a moderate Reynolds number to develop improved formulas for friction and heat transfer prediction.

2. Methodology

We solve the compressible Navier–Stokes equations using our flow solver STREAmS (Bernardini *et al.* 2021, 2023). The streamwise momentum equation is forced in such a way as to maintain a constant mass flow rate. Periodicity is exploited in the streamwise and spanwise directions, and isothermal no-slip boundary conditions are used at the channel walls. Let h be the half-width of the channel, the DNS have been carried out in a computational domain $L_x \times L_y \times L_z = 6\pi h \times 2h \times 2\pi h$. A uniform bulk cooling or heating term is added to the energy equation to guarantee that the mixed mean temperature, defined as,

$$T_m = \frac{1}{2h\rho_b u_b} \int_0^{2h} \bar{\rho} \bar{u} \bar{T} dy, \quad \rho_b = \frac{1}{2h} \int_0^{2h} \bar{\rho} dy, \quad u_b = \frac{1}{2h\rho_b} \int_0^{2h} \bar{\rho} \bar{u} dy, \quad (2.1)$$

remains exactly constant in time. Here, ρ_b and u_b are the bulk density and velocity, respectively. In the following, the overline symbol is used to indicate Reynolds averaging in time and in the homogeneous spatial directions, and the prime superscript is used to denote fluctuations thereof. As common in variable-density flows, we also use Favre averages, denoted with the tilde superscript $\tilde{f} = \overline{\rho f} / \bar{\rho}$, and the double prime superscript will indicate fluctuations thereof.

The + superscript is used to denote normalization by wall units, namely by friction velocity, $u_\tau = (\tau_w / \bar{\rho}_w)^{1/2}$ (where $\tau_w = \mu_w d\bar{u}/dy|_w$ is the mean wall shear stress), and the associated viscous length scale, $\delta_v = \nu_w / u_\tau$, where the subscript 'w' denotes quantities evaluated at the wall. For inner normalization of the mean temperature, we use the friction temperature, $\theta_\tau = q_w / (\rho_w c_p u_\tau)$, where $q_w = \lambda_w d\bar{T}/dy|_w$ is the mean wall heat flux, where $c_p = \gamma / (\gamma - 1)R$ is the specific heat capacity at constant pressure, R the air constant, and λ_w is the thermal conductivity at the wall, evaluated as $\lambda = \mu c_p / Pr$, with Prandtl number set to $Pr = 0.72$.

Twenty DNS have been carried out at bulk Mach number $M_b = u_b / c_m = 0.2$ (where c_m is the speed of sound at the mixed mean temperature), and bulk Reynolds number $Re_b = 2\rho_b u_b h / \mu_m \approx 9000\text{--}70000$ (see table 1), where $\mu_m = \mu(T_m)$ is the dynamic viscosity evaluated at the mixed mean temperature, as obtained from Sutherland's law (White 1974). The Mach number is low enough that compressibility effects are negligible, as it turns out, in order to isolate variable-property effects. We consider various mean-to-wall

	Re_b	Re_τ	T_m/T_w	T_w (K)	Re_τ^*	$C_f \times 10^3$	$St \times 10^3$	Nu	N_x	N_y	N_z	Δx^*	$\Delta y_w^* - \Delta y_{max}^*$	Δz^*
L04	17182	155	0.4	800	533	5.45	3.09	38.3	1024	280	512	9.8	0.69–5.1	6.5
L05-A	20170	212	0.5	293.15	612	5.57	3.18	46.2	1024	280	512	11.3	0.67–5.9	7.5
L05-B	17115	205	0.5	800	511	5.62	3.21	39.5	1024	280	512	9.4	0.58–4.9	6.3
L07	13565	255	0.7	800	400	6.28	3.56	34.8	1024	280	512	7.4	0.40–3.8	4.9
L08	16679	356	0.8	800	470	6.01	3.4	40.9	1024	280	512	8.7	0.47–4.5	5.8
L15	14632	663	1.5	800	406	6.82	4.1	43.2	1024	280	512	7.5	0.41–3.9	5
L2	11389	789	2	293.15	317	7.31	4.37	35.9	1024	280	512	5.8	0.32–3.0	3.9
L25	9853	902	2.5	293.15	278	7.75	4.62	32.8	1024	280	512	5.1	0.28–2.7	3.4
L3	9212	1051	3	293.15	261	8.04	4.78	31.7	1024	280	512	4.8	0.18–2.5	3.2
H04	31797	260	0.4	800	893	4.52	2.59	59.3	2048	480	1024	8.2	0.66–5.0	5.5
H07	37887	617	0.7	800	971	4.75	2.73	74.5	2048	480	1024	8.9	0.45–5.4	6
H05-A	37589	360	0.5	293.15	1040	4.66	2.68	72.5	2048	480	1024	9.6	0.37–5.8	6.4
H05-B	37933	404	0.5	800	1007	4.47	2.57	70.3	2048	480	1024	9.3	0.57–5.6	6.2
H08	34703	674	0.8	800	890	4.97	2.83	70.7	2048	480	1024	8.2	0.41–5.0	5.5
H15	18694	861	1.5	293.15	498	6.3	3.78	50.8	2048	480	1024	4.6	0.27–2.8	3.1
H2	15362	1028	2	293.15	415	6.81	4.06	44.9	2048	480	1024	3.8	0.15–2.3	2.5
H25	13873	1224	2.5	293.15	378	7.15	4.26	42.5	2048	480	1024	3.5	0.13–2.1	2.3
H3	12898	1420	3	293.15	354	7.44	4.42	41.1	2048	480	1024	3.3	0.12–2.0	2.2
VH05	68874	680	0.5	800	1687	3.85	2.22	110.3	4096	800	2048	7.8	0.30–5.6	5.2
VH2	54439	3201	2	293.15	1298	5.22	3.13	122.9	4096	800	2048	6	0.23–4.3	4

Table 1: Flow parameters for plane channel flow DNS. Box dimensions are $6\pi h \times 2h \times 2\pi h$ for all flow cases. $Re_b = 2\rho_b h u_b/\nu_m$ is the bulk Reynolds number and $Re_\tau = h u_\tau/\nu_w$ is the friction Reynolds number. $Re_{\tau_{cp}} = y_{cp}(h)/\delta_v$ is the equivalent friction Reynolds number. T_m and T_w are the mixed mean temperature and the wall temperature, respectively. $C_f = 2\tau_w/(\rho_b u_b^2)$ is the friction coefficient, St is the Stanton number and Nu is the Nusselt number. Δx and Δz are the mesh spacing in the streamwise and spanwise directions, and Δy_w is the mesh spacing at the wall, all given in equivalent constant-properties wall units, $u_\tau, c_p, \delta_v, c_p$, defined in equation (4.15).

temperature ratios, namely $T_m/T_w = [0.4, 0.5, 0.7, 0.8, 1.5, 2, 2.5, 3]$, resulting in friction Reynolds numbers in the range $Re_\tau = u_\tau h/\nu_w \approx 150\text{--}3200$, where ν_w is the kinematic viscosity at the wall. For two flow cases with mean-to-wall temperature ratio $T_m/T_w = 0.5$ and $T_m/T_w = 2$ we also consider a ‘very high’ Reynolds number case, denoted with VH. For the case of mean-to-wall temperature ratio $T_m/T_w = 0.5$, we also study the effect of varying the dimensional wall temperature, considering cases with $T_w = 800K$ and $T_w = 293.15K$. For each value of the mean-to-wall temperature ratio, we have two flow cases denoted with the letter L or H, depending on whether the Reynolds number is comparatively ‘low’ or ‘high’.

3. Instantaneous temperature field

We begin our analysis by inspecting the instantaneous velocity and temperature fields of flow cases H05 and H3 in figure 1. Both cases exhibit the qualitative features that characterize wall turbulence, with high-speed cold (or hot) flow structures protruding towards the walls, and low-speed hot (or cold) fluid regions protruding towards the channel center. Despite sharing the general features of wall turbulence, we also note a significant effect of the thermodynamic and fluid property variations between cases with wall heating and wall cooling. First, we observe that the friction Reynolds number values reported in table 1 are not indicative of actual separation of scales in constant-property flows, as for instance flow case H05 has lower friction Reynolds number while exhibiting finer eddies. This effect can be traced to strong viscosity variations within the near-wall and core flow regions. The cooled flow case H3 indeed appears to be a ‘filtered’ version of the heated case, in which only large structures survive. In fact, in flow case H3 we observe large structures extending from one wall to beyond the channel centreline, whereas those are masked by smaller eddies in flow case H05.

We note that the instantaneous velocity and temperature fields are highly correlated, which is to be expected due to the similarity of the underlying equations and the near-unity value of the Prandtl number, hence Reynolds analogy qualitatively holds also for the case of variable fluid properties. Close scrutiny of the kinematic and thermal fields reveals that temperature has finer structures as compared to velocity, which is partially due to Prandtl number being lower than unity and partially to the absence of the pressure gradient in the temperature equation (Pirozzoli *et al.* 2016).

4. Mean flow field and variable-properties transformations

We begin the mean flow analysis by comparing the mean velocity and temperature profiles to the equivalent statistics for the constant property case. For that purpose we rely both on DNS data of constant-properties plane channel flow with passive scalar transport at $Pr = 0.71$ from Pirozzoli *et al.* (2016), and on synthetic composite profiles, which are obtained by matching inner-layer velocity and temperature profiles with the corresponding outer-layer distributions. The inner-layer profiles are obtained by integrating the eddy viscosity of Musker (1979) for the velocity and the eddy diffusivity proposed by Pirozzoli (2023) for the temperature profile. In the outer layer we use Clauser’s hypothesis of uniform eddy viscosity (Pirozzoli 2014) and uniform eddy diffusivity (Pirozzoli *et al.* 2016). A complete derivation of the composite profiles is available in Pirozzoli & Modesti (2024). Figure 2 shows that the composite profiles of mean temperature and velocity for the constant-property case are essentially indistinguishable from the DNS data, with the advantage that the synthetic profiles are available at any Reynolds and Prandtl number.

We note that the statistics of the variable-properties DNS are substantially different from the constant-properties case when scaled in classical wall units. All the flow cases exhibit

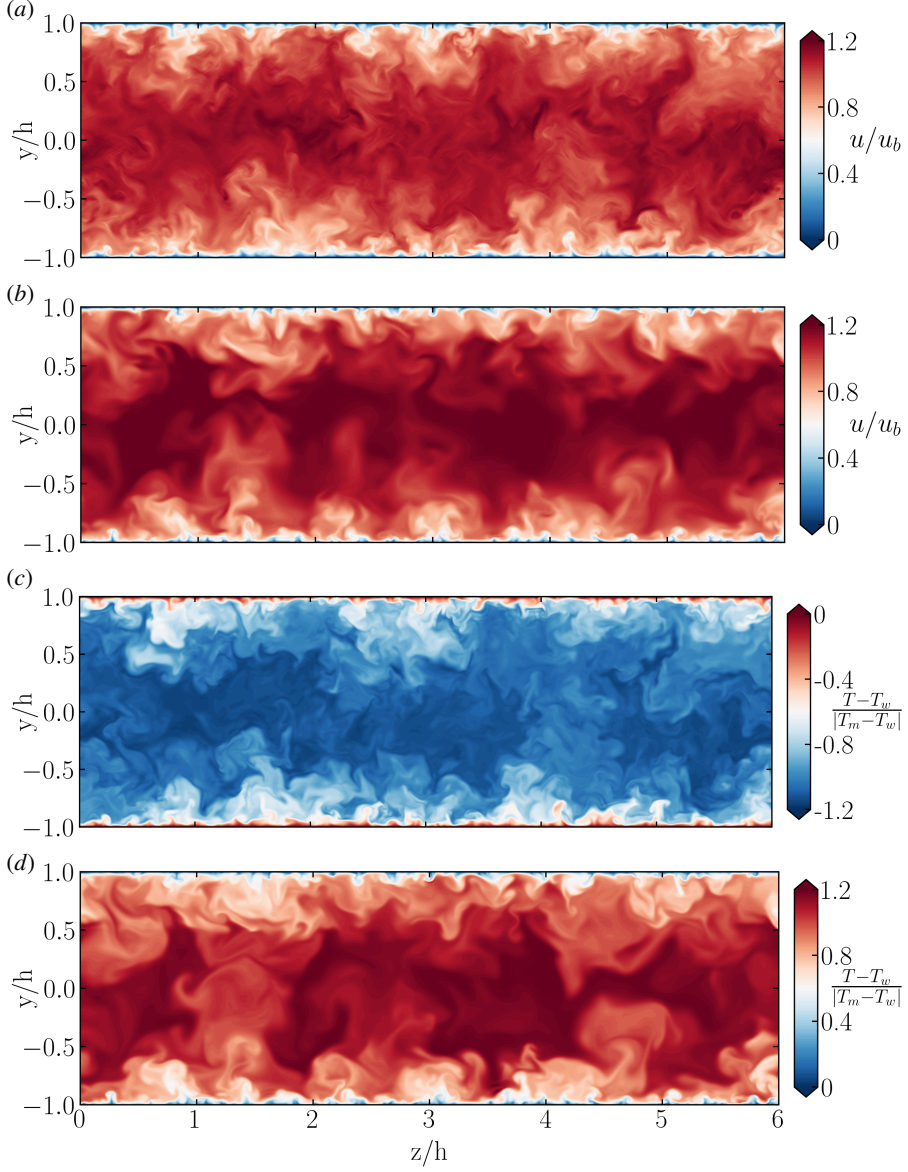


Figure 1: Instantaneous velocity (a,b) and temperature (c,d) fields in a cross-stream plane, for flow case H05 (a,c) and H3 (b,d).

deviations from the reference, starting from the buffer region, and becoming more evident in the logarithmic region, where both the logarithmic slope and the additive constant deviate from the constant-properties references. Hence, we conclude that in the variable-properties case the law-of-the-wall for both the mean velocity and temperature is not universal, but rather depends on the specific mean-to-wall-temperature ratio.

In analogy with what done in compressible flows, we assume that the effects of density and viscosity variations can be accounted for using suitable convolution integrals (Modesti

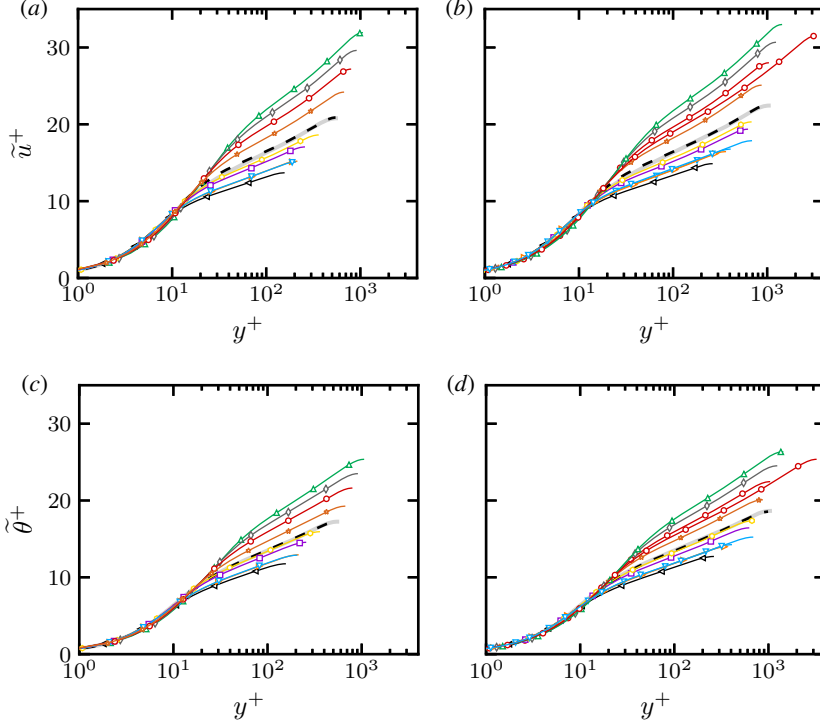


Figure 2: Mean velocity (*a,b*) and mean temperature (*c,d*) profiles for L flow cases (*a,c*) and H flow cases (*b,d*). Symbols indicate DNS data for different mean-to-wall temperature ratios: $T_m/T_w = 0.4$ (left triangles), $T_m/T_w = 0.5$, $T_w = 800K$ (downward triangle), $T_m/T_w = 0.5$, $T_w = 273.25K$ (right triangles), $T_m/T_w = 0.7$ (squares), $T_m/T_w = 0.8$ (hexagons), $T_m/T_w = 1.5$ (stars), $T_m/T_w = 2$ (circles), $T_m/T_w = 2.5$ (diamonds), $T_m/T_w = 3$ (upward triangles). Gray solid lines indicate the mean velocity and temperature profiles of the constant properties case, obtained using the synthetic velocity profile of Musker (1979) and the synthetic temperature profile of Pirozzoli (2023).

& Pirozzoli 2016),

$$y_{cp} = \int_0^y f_{cp} dy, \quad u_{cp} = \int_0^{\tilde{u}} g_{cp} d\tilde{u}, \quad \theta_{cp} = \int_0^{\tilde{\theta}} h_{cp} d\tilde{\theta}, \quad (4.1)$$

with kernel functions f_{cp} , g_{cp} , h_{cp} to be specified such that the flow properties are mapped to the universal, constant-properties case, denoted with the ‘cp’ subscript. In order to account for variable-properties effect, we consider the streamwise mean momentum balance equation,

$$\overline{\mu' \frac{du'}{dy}} + \bar{\mu} \frac{d\tilde{u}}{dy} - \overline{\rho u'' v''} = \bar{\rho}_w u_\tau^2 (1 - \eta), \quad (4.2)$$

where $\eta = y/h$. Following Hasan *et al.* (2023), we then introduce an eddy viscosity for the turbulent shear stress, such that $-\overline{\rho u'' v''} = \bar{\rho} \nu_T d\tilde{u}/dy$. Substituting the transformations (4.1) into the streamwise mean momentum balance equation, and assuming $\overline{\mu' du'/dy} \approx 0$, one obtains

$$\frac{\bar{\mu}}{\mu_w} \frac{f_{cp}}{g_{cp}} \left(1 + \frac{\nu_T}{\nu} \right) \frac{du_{cp}^+}{dy_{cp}^+} = 1 - \eta. \quad (4.3)$$

Comparing equation (4.3) with the constant-properties counterpart,

$$\left(1 + \frac{\nu_{T,cp}}{\nu}\right) \frac{du_{cp}^+}{dy_{cp}^+} = 1 - \eta, \quad (4.4)$$

and assuming that the kernel function f_{cp} is the same as in Trettel & Larsson (2016), we can also determine g_{cp} ,

$$f_{cp} = \frac{d}{dy} \left(\frac{y}{R^{1/2}N} \right), \quad g_{cp} = \left(\frac{1 + \nu_T/\nu}{1 + \nu_{T,cp}/\nu} \right) RN \frac{d}{dy} \left(\frac{y}{R^{1/2}N} \right), \quad (4.5)$$

where $N = \bar{\nu}/\nu_w$, $R = \bar{\rho}/\bar{\rho}_w$. The kernel functions (4.5) are formally equivalent to the velocity transformation derived by Hasan *et al.* (2023) for high-speed turbulent boundary layer, with eddy viscosities to be specified. Using the model eddy viscosity of Musker (1979) for the baseline case of constant-properties flow, herein we extend the model to account for variable-properties effects by including an ad-hoc correction depending on the mean-to-wall temperature ratio

$$\frac{\nu_{T,cp}}{\nu} = \frac{(\kappa y_{cp}^+)^3}{(\kappa y_{cp}^+)^2 + C_{v1}^2}, \quad \frac{\nu_T}{\nu} = \frac{(\kappa y_{cp}^+)^3}{(\kappa y_{cp}^+)^2 + C_{v1}^2 + \varphi(T_m/T_w)}, \quad (4.6)$$

where $\kappa = 0.387$ is the assumed Kármán constant, and $C_{v1} = 7.3$. Fitting the present DNS data (only flow cases at 'high Reynolds numbers', denoted as H, have been taken into account) we have determined empirically the following expressions for the additive function φ ,

$$\varphi(T_m/T_w) = \begin{cases} 32 \log(T_m/T_w) - 52(1 - T_m/T_w)^2, & T_m/T_w < 1 \\ 5.6(1 - T_m/T_w), & T_m/T_w > 1. \end{cases} \quad (4.7)$$

Similarly to what done for the mean velocity, a transformation for the mean temperature profile is obtained starting from the mean energy balance equation,

$$\underbrace{\lambda' \frac{d\theta'}{dy}}_{\text{Fluctuating Conduction}} + \underbrace{\bar{\lambda} \frac{d\bar{\theta}}{dy}}_{\text{Mean Conduction}} + \underbrace{-C_p \bar{\rho} \overline{\theta'' v''}}_{\text{Turbulent Convection}} + \underbrace{\Psi}_{\text{Dissipation}} = \underbrace{q_w}_{\text{Total heat flux}} (1 - \mathcal{R}), \quad (4.8)$$

where

$$\mathcal{R}(\eta) = \frac{1}{\rho_b} \int_0^\eta \bar{\rho}(\eta) d\eta, \quad \Psi = \int_0^y \epsilon dy - \int_0^y \frac{\rho}{\rho_b} \int_0^1 \epsilon d\eta dy, \quad \epsilon = \overline{\sigma_{ij} \frac{\partial u_i}{\partial x_j}} - \overline{u_i \frac{\partial p}{\partial x_i}}. \quad (4.9)$$

The relative importance of the different terms in equation (4.8) is analysed in figure 3, for representative flow cases with wall heating and wall cooling. Figure 3 shows that the mean temperature balance of variable-properties flows is qualitatively similar to what found in passive scalar convection, with mean conduction dominating the near-wall region and turbulent convection dominating the overall balance away from the wall. However, notable differences are the nonlinearity of the total heat flux (on account of the definition of \mathcal{R}) and the presence of additional terms which are small but not zero. Indeed, very close to the wall we find small contribution of the fluctuating conduction term, which however remains much smaller than the mean conduction. The dissipation remains a negligible contribution for all cases considered here, due to the small Mach number under scrutiny, confirming that all flow cases can be regarded as representative of incompressible flow.

Based on the DNS data, we then assume $\Psi \approx 0$ and $\overline{\lambda' d\theta'/dy} \approx 0$ and, in analogy with

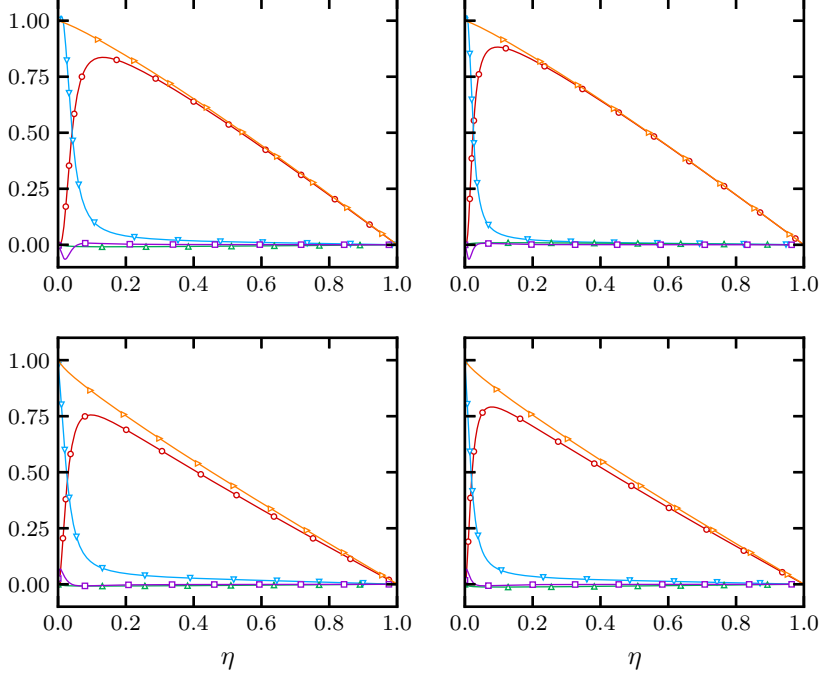


Figure 3: Mean energy balance as in equation (4.8) for flow cases L05 (a), H05 (b), L3 (c), and H3 (d). The symbols indicate mean conduction (downward triangles), fluctuating conduction (squares), turbulent convection (circles), dissipation (upward triangles), total heat flux(right triangles).

what done for the turbulent shear stress, we model the turbulent heat flux by introducing a thermal eddy diffusivity, such that

$$\widetilde{\theta''v''} \frac{(1-\eta)}{(1-\mathcal{R})} = -\alpha_T \frac{d\tilde{\theta}}{d\eta}. \quad (4.10)$$

Following the same procedure used for the mean momentum equation, we then determine the corresponding kernel function,

$$h_{cp} = \left(\frac{1 + \alpha_T/\alpha}{1 + \alpha_{T,cp}/\alpha} \right) \frac{(1-\eta)}{(1-\mathcal{R})} RN \frac{d}{d\eta} \left(\frac{y}{R^{1/2}N} \right), \quad (4.11)$$

where $\alpha = \lambda/(\rho c_p)$ is the thermal diffusivity coefficient. Following Pirozzoli (2023), we model the turbulent diffusivity as follows,

$$\frac{\alpha_{T,cp}}{\alpha} = \frac{(\kappa_\theta y_{cp}^+)^3}{(\kappa_\theta y_{cp}^+)^2 + C_{v3}^2}, \quad \frac{\alpha_T}{\alpha} = \frac{(\kappa_\theta y_{cp}^+)^3}{(\kappa_\theta y_{cp}^+)^2 + C_{v3}^2 + \beta(T_m/T_w)} \quad (4.12)$$

with constants $\kappa_\theta = 0.459$, $C_{v3} = 10$. As for the mean velocity, the dependency of the eddy thermal diffusivity on mean-to-wall temperature ratio is empirically accounted for by fitting

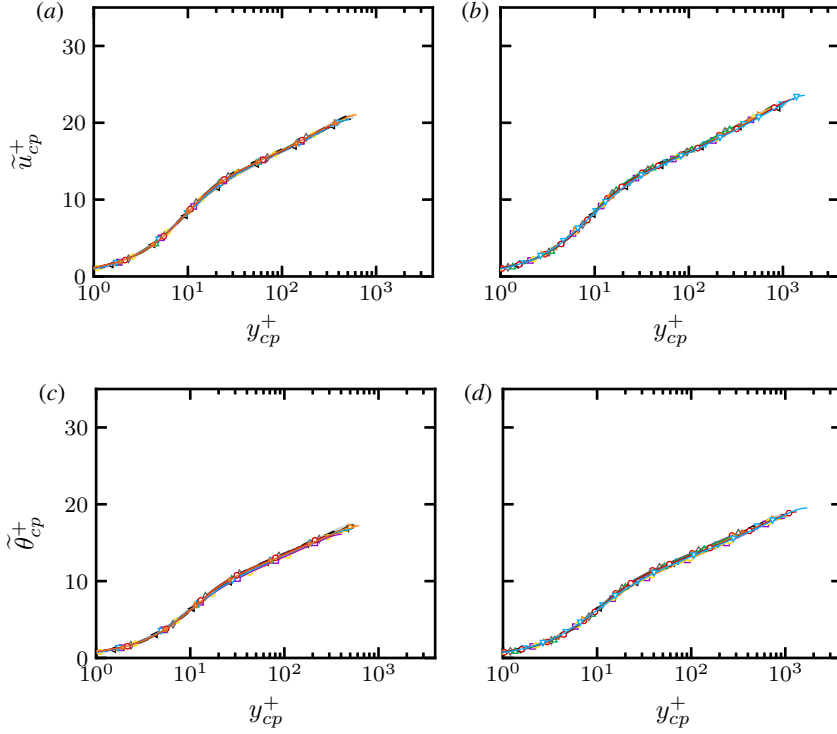


Figure 4: Mean velocity (a,b) and mean temperature (c,d) profiles transformed using equation (4.1) with kernel functions (4.5) and (4.12), for L flow cases (a,c) and H flow cases (b,d). Symbols indicate DNS data for different mean-to-wall temperature ratios: $T_m/T_w = 0.4$ (left triangles), $T_m/T_w = 0.5, T_w = 800K$ (downward triangles), $T_m/T_w = 0.5, T_w = 273.25K$ (right triangles), $T_m/T_w = 0.7$ (squares), $T_m/T_w = 0.8$ (hexagons), $T_m/T_w = 1.5$ (stars), $T_m/T_w = 2$ (circles), $T_m/T_w = 2.5$ (diamonds), $T_m/T_w = 3$ (upward triangles). The gray solid lines indicate the reference mean velocity and temperature profiles of the constant-properties case, obtained using the synthetic velocity profile of Musker (1979) and the synthetic temperature profile of Pirozzoli (2023).

the DNS data, to obtain

$$\beta(T_m/T_w) = \begin{cases} (1 - T_m/T_w)[700(T_m/T_w)^2 - 1700(T_m/T_w)^3 + 1500(T_m/T_w)^4], & T_m/T_w < 1 \\ -28 \log(T_m/T_w) + 2.2(1 - T_m/T_w)^2, & T_m/T_w > 1. \end{cases} \quad (4.13)$$

We note that both equations (4.7) and (4.13) show different functional dependency for heating and cooling, which is aligned with empirical formulas for the Nusselt number and friction coefficient reported in the literature (Petukhov 1970; Yeh & Stepka 1984), featuring different coefficients or functions for the two cases.

In figure 4, we plot the transformed mean velocity and temperature profiles using the kernel functions (4.5) and (4.12), and compare the results with the reference constant-properties case. The universality of the various distributions is quite remarkable, given the wide range of variation of the flow properties which we are considering. The accuracy of the velocity and temperature transformations also supports the validity of the assumptions made to derive the kernel functions for the convolution integrals (4.1). We point out that the coefficients inferred from DNS have been calibrated only for flow cases H, and the are successfully applied to

lower or higher Reynolds number with similar accuracy, showing substantial independence from the Reynolds number. These transformations allow us to define an equivalent channel height h_{cp} , which we use to introduce an equivalent constant-properties friction Reynolds number,

$$Re_{\tau,cp} = \frac{h_{cp}}{\delta_v}, \quad h_{cp} = \int_0^h f_{cp} dy. \quad (4.14)$$

The equivalent channel height h_{cp} is larger than h for heating and smaller for cooling, leading to higher or lower equivalent constant-properties friction Reynolds number, respectively. The definition given in equation (4.14), can also be used to define an equivalent constant-properties friction velocity, and an equivalent viscous length scale, namely

$$Re_{\tau,cp} = \frac{u_{\tau,cp} h}{\bar{v}_w}, \quad u_{\tau,cp} = \frac{\bar{v}_w}{\delta_{v,cp}}, \quad \delta_{v,cp} = \frac{h}{h_{cp}} \delta_v \quad (4.15)$$

Values of the equivalent constant-properties Reynolds numbers are reported in table 1, which can be used as a guideline to interpret the instantaneous flow field in figure 1, where flow cases with heating show finer eddies than for cooling because their effective Reynolds number is higher.

5. Wall friction and heat transfer

The variable-properties transformations developed in the previous section are very useful especially as they enable the prediction of the heat transfer and friction coefficients. For that purpose, the only required inputs are the reference constant-property mean velocity and mean temperature profiles. As previously discussed, in the current work we consider the composite profiles developed in the work of Pirozzoli (2014) and Pirozzoli & Modesti (2024). However, different choices are possible, and one could for instance use the model for the mean velocity by Nagib & Chauhan (2008), and the model for the mean temperature by Kader (1981), although the latter might result in less accurate temperature profiles due to inconsistencies in the near-wall region. Starting from those, application of the inverse of transformations (4.1) allows us to determine the actual variable-properties profiles, for any given mean-to-wall temperature ratio and Reynolds number. The key technical difficulty is that the kernel functions f_{cp} , g_{cp} , h_{cp} depend on the actual temperature in the variable-property case, hence an iterative procedure is necessary, as for compressible flow (Kumar & Larsson 2022; Hasan *et al.* 2024). The iterative procedure is presented in 1 and it can be summarized as follows,

- 1 Generate the constant properties profiles for a target friction Reynolds number $Re_{\tau,cp}$
- 2 Initialize kernel functions f_{cp} , g_{cp} , h_{cp} using the constant-properties temperature profile
- 3 Calculate the backward convolution integrals (4.1) to find y , u , θ
- 4 Update the kernels f_{cp} , g_{cp} , h_{cp}
- 5 Calculate the friction coefficient, Stanton number and $Re_{\tau,cp}$
- 6 Update the constant properties profiles based on the updated $Re_{\tau,cp}$.

Note that two nested loops are required for this iterative algorithm. This is because the constant properties profiles are also re-calculated at each step in order to converge towards the target friction Reynolds number $Re_{\tau,cp}$.

Figure 5 shows the resulting friction coefficient $C_f = 2\tau_w/(\rho_b u_b^2)$, and the Stanton number $St = q_w/[\rho_b C_p u_b (T_w - T_m)]$. Whereas the data for the constant-properties case (black pentagons) fall on top of the corresponding theoretical curves (light gray), we find significant deviations thereof in cases with properties variations. In particular, we note that

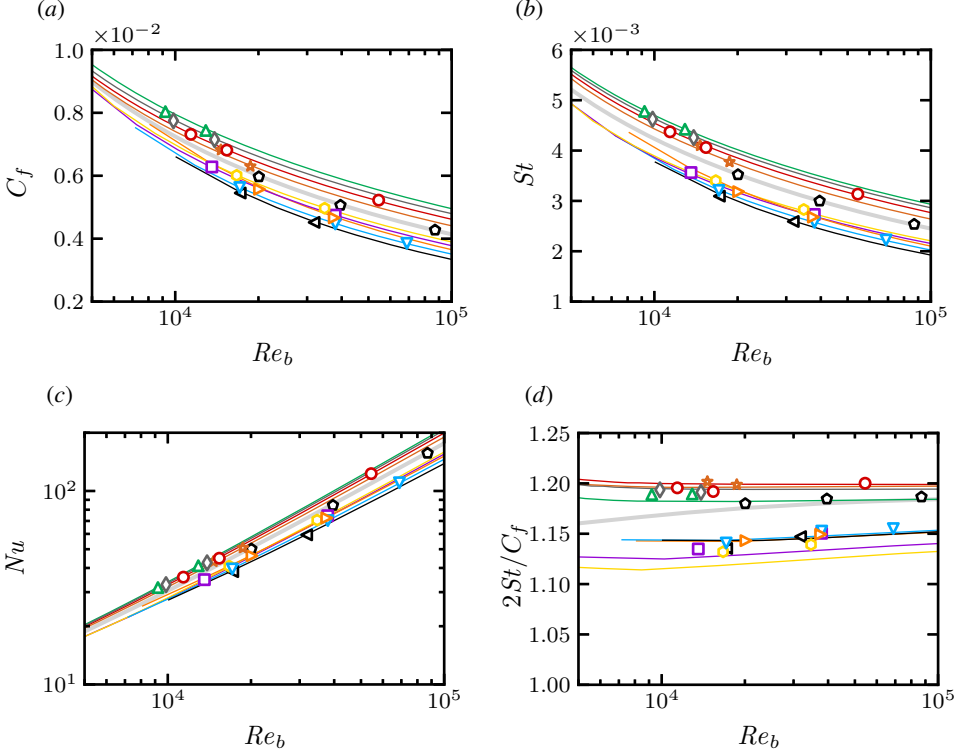


Figure 5: Friction coefficient (a), Stanton number (b), Nusselt number (c) and Reynolds analogy factor (d) as a function of the bulk Reynolds number $Re_b = 2h\rho_b u_b / \mu_m$. Solid lines indicate predictions obtained by inverting the variable-properties transformations (4.1), and symbols indicate DNS data for different mean-to-wall temperature ratios, with matching colors: $T_m/T_w = 0.4$ (black left triangles), $T_m/T_w = 0.5, T_w = 800K$ (orange downward triangle), $T_m/T_w = 0.5, T_w = 273.25K$ (blue right triangles), $T_m/T_w = 0.7$ (purple squares), $T_m/T_w = 0.8$ (gold hexagons), $T_m/T_w = 1.5$ (brown stars), $T_m/T_w = 2$ (red circles), $T_m/T_w = 2.5$ (dark gray diamonds), $T_m/T_w = 3$ (green upward triangles).

cases with heated wall yield reduced friction and heat flux, whereas cases with cooled wall yield an increase of momentum and heat transfer, with a scatter around the constant-properties case of $\pm 25\%$ for both the friction coefficient and the Stanton number. We also report the heat transfer in terms of Nusselt number $Nu = Re_b St Pr$, although this representation tends to hide differences within a few percent, thus the Stanton number should be preferred for accurate evaluation of theories. Theoretical predictions relying on use of the variable-properties transformations (4.1) are shown in the figure with solid line of matching colors, and of course those are not universal as well. Notably, figure 5 shows that the resulting predictions match the DNS data to within 1-2% accuracy for all cases, both for the friction and heat transfer coefficients, as shown quantitatively in figure 6. We further find that the analogy between momentum and heat transfer holds also in the case of variable-properties flows, as the Reynolds analogy factor stays close to unity for all the flow cases, although this information alone is obviously not sufficient to recover the heat transfer and friction coefficients from the constant-properties case.

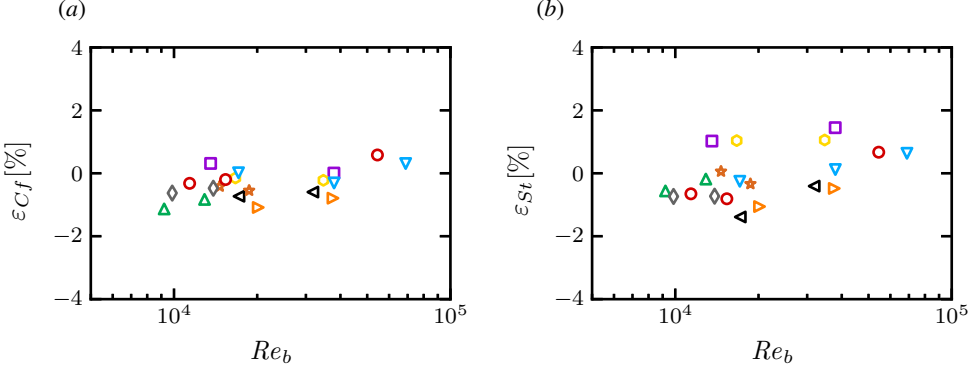


Figure 6: Percent difference between DNS data and predicted friction coefficient (a) and Stanton number (b) as a function of the bulk Reynolds number $Re_b = 2h\rho_b u_b / \mu_m$. Symbols indicate DNS data for different mean-to-wall temperature ratios: $T_m/T_w = 0.4$ (left triangles), $T_m/T_w = 0.5, T_w = 800K$ (downward triangle), $T_m/T_w = 0.5, T_w = 273.25K$ (right triangles), $T_m/T_w = 0.7$ (squares), $T_m/T_w = 0.8$ (hexagons), $T_m/T_w = 1.5$ (stars), $T_m/T_w = 2$ (circles), $T_m/T_w = 2.5$ (gray diamonds), $T_m/T_w = 3$ (upward triangles).

Algorithm 1 Inverse variable properties transformation

Initialization:

- 1: Generate constant properties profiles at $Re_{\tau, cp \text{ target}}: u_{cp}^n, \theta_{cp}^n$
- 2: Set: $u^n = u_{cp}^n, \theta^n = \theta_{cp}^n$, Calculate: $f_{cp}^n, g_{cp}^n, h_{cp}^n, C_f^n, St^n$

while ($|Re_{\tau, cp}^n - Re_{\tau, cp \text{ target}}| < tol$) **do**

while ($|C_f^{n+1} - C_f^n| < tol$) **and** ($|St^{n+1} - St^n| < tol$) **do**

3: $y^{n+1} = \int \frac{1}{f_{cp}^n} dy_{cp}^n, \quad u^{n+1} = \int \frac{1}{g_{cp}^n} du_{cp}^n, \quad \theta^{n+1} = \int \frac{1}{h_{cp}^n} d\theta_{cp}^n$

4: Update kernels: $f_{cp}^{n+1}, g_{cp}^{n+1}, h_{cp}^{n+1}$

5: Update coefficients and Reynolds: $C_f^{n+1}, St^{n+1}, Re_{\tau, cp}^{n+1}$

6: Update constant properties profiles $u_{cp}^{n+1}, \theta_{cp}^{n+1}$ at $Re_{\tau, cp}^{n+1}$

end while

end while

6. Conclusions

Currently, predicting heat transfer through forced convection in real fluids heavily depends on fitting experimental data obtained decades ago, leading to uncertainties of up to 20-30%. This significant variability is clearly reflected in the current DNS data. To address this uncertainty, we have developed a robust framework for estimating momentum and heat transfer coefficients. Our approach is grounded in the first principles of momentum and energy balance rather than empirical methods, offering the advantages of accuracy and

generalizability. Similar to approaches used in high-speed turbulent boundary layers, our method relies on transformation kernels for velocity and temperature distributions.

Preliminary tests indicate that transformation kernels informed by DNS data can generate velocity and temperature distributions with excellent universality compared to the constant-property case. Evaluating momentum and heat transfer coefficients involves integrating the estimated velocity and temperature profiles obtained through the backward application of these transformation kernels, requiring an iterative procedure. Our results indicate that the method can accurately predict heat transfer and friction coefficients within 1-2% compared to DNS data. Additionally, the developed method can determine mean temperature and velocity profiles alone, providing valuable information for establishing wall functions in simulations employing wall-modeled approaches.

We also acknowledge that cooling ducts in practical applications often feature rough walls rather than smooth ones (Chung *et al.* 2021; Zhong *et al.* 2023; De Maio *et al.* 2023). This raises questions about the applicability of the current transformations to complex surface patterns. In such cases, the effects of density and viscosity variations lead to a much more intricate flow physics compared to constant-properties flows. Several mechanisms and parameters remain to be studied, including the precise mechanisms responsible for friction and heat transfer variation, the impact on turbulence length scales, and the influence of the working fluid. We plan to investigate these aspects in future studies.

Acknowledgements

We acknowledge CHRONOS for awarding us access to Piz Daint, at the Swiss National Supercomputing Centre (CSCS), Switzerland. We also acknowledge EuroHPC for access to LEONARDO based at CINECA, Casalecchio di Reno, Italy.

REFERENCES

- ABE, H. & ANTONIA, R.A. 2017 Relationship between the heat transfer law and the scalar dissipation function in a turbulent channel flow. *J. Fluid Mech.* **830**, 300–325.
- ALCÁNTARA-ÁVILA, F., HOYAS, S. & PÉREZ-QUILES, M.J. 2021 Direct numerical simulation of thermal channel flow for $Re_\tau = 5000$ and $Pr = 0.71$. *J. Fluid Mech.* **916**.
- BERNARDINI, M., MODESTI, D., SALVADORE, F. & PIROZZOLI, S. 2021 STREAmS: A high-fidelity accelerated solver for direct numerical simulation of compressible turbulent flows. *Comput. Phys. Commun.* **263**, 107906.
- BERNARDINI, M., MODESTI, D., SALVADORE, F., SATHYANARAYANA, S., POSTA, G. DELLA & PIROZZOLI, S. 2023 STREAmS-2.0: Supersonic turbulent accelerated Navier–Stokes solver version 2.0. *Comput. Phys. Commun.* **285**, 108644.
- CEBECI, T. 1973 A model for eddy conductivity and turbulent Prandtl number. *Int. J. Heat Mass Transf.* **95**, 227–234.
- CHUNG, D., HUTCHINS, N., SCHULTZ, M. P. & FLACK, K.A. 2021 Predicting the drag of rough surfaces. *Annu. Rev. Fluid Mech.* **53**, 439–471.
- DE MAIO, M., LATINI, B., NASUTI, F. & PIROZZOLI, S. 2023 Direct numerical simulation of turbulent flow in pipes with realistic large roughness at the wall. *J. Fluid Mech.* **974**, A40.
- DITTUS, F.W. & BOELTER, L.M.K. 1933 Heat transfer in automobile radiators of the tubular type. *Int. Commun. Heat Mass Transf.* **12**, 3–22.
- DITTUS, F.W. & BOELTER, L.M.K. 1985 Heat transfer in automobile radiators of the tubular type. *Int. Commun. Heat Mass Transf.* **12** (1), 3–22.
- GNIELINSKI, V. 1976 New equations for heat and mass transfer in turbulent pipe and channel flow. *Int. Chem. Eng.* **16**, 359–367.
- HASAN, A.M., LARSSON, J., PIROZZOLI, S. & PECNIK, R. 2023 Incorporating intrinsic compressibility effects in velocity transformations for wall-bounded turbulent flows. *Physical Review Fluids* **8** (11), L112601.
- HASAN, A.M., LARSSON, J., PIROZZOLI, S. & PECNIK, R. 2024 Estimating Mean Profiles and Fluxes in High-Speed Turbulent Boundary Layers Using Inner/Outer-Layer Scalings. *AIAA J.* **62** (2), 848–853.

- INCROPERA, FRANK P, DEWITT, DAVID P, BERGMAN, THEODORE L, LAVINE, ADRIENNE S & OTHERS 1996 *Fundamentals of heat and mass transfer*, , vol. 6. Wiley New York.
- KADER, B.A. 1981 Temperature and concentration profiles in fully turbulent boundary layers. *Int. J. Heat Mass Transf.* **24** (9), 1541–1544.
- KAKAC, S., LIU, H. & PRAMUANJAROENKIJ, A. 2002 *Heat exchangers: selection, rating, and thermal design*. CRC press.
- KALLER, T., PASQUARIELLO, V., HICKEL, S. & ADAMS, N.A. 2019 Turbulent flow through a high aspect ratio cooling duct with asymmetric wall heating. *J. Fluid Mech.* **860**, 258–299.
- KUMAR, V. & LARSSON, J. 2022 Modular method for estimation of velocity and temperature profiles in high-speed boundary layers. *AIAA J.* **60** (9), 5165–5172.
- LEE, J., JUNG, S.Y., SUNG, H.J. & ZAKI, T.A. 2013 Effect of wall heating on turbulent boundary layers with temperature-dependent viscosity. *J. Fluid Mech.* **726**, 196–225.
- LEE, J., JUNG, S.Y., SUNG, H.J. & ZAKI, T.A. 2014 Turbulent thermal boundary layers with temperature-dependent viscosity. *Int. J. Heat Fluid Flow* **49**, 43–52.
- MODESTI, D. & PIROZZOLI, S. 2016 Reynolds and Mach number effects in compressible turbulent channel flow. *Int. J. Heat Fluid Flow* **59**, 33–49.
- MUSKER, A.J. 1979 Explicit expression for the smooth wall velocity distribution in a turbulent boundary layer. *AIAA J.* **17** (6), 655–657.
- NAGIB, H.M. & CHAUHAN, K.A. 2008 Variations of von Kármán coefficient in canonical flows. *Phys. Fluids* **20** (10).
- NIKURADSE, J. 1933 Stromungsgesetze in rauhen Rohren. *vti-forschungsheft* **361**, 1.
- PATEL, A., BOERSMA, B.J. & PECNIK, R. 2016 The influence of near-wall density and viscosity gradients on turbulence in channel flows. *J. Fluid Mech.* **809**, 793–820.
- PATEL, A., BOERSMA, B.J. & PECNIK, R. 2017 Scalar statistics in variable property turbulent channel flows. *Phys. Rev. Fluids* **2** (8), 084604.
- PETUKHOV, B.S. 1970 Heat transfer and friction in turbulent pipe flow with variable physical properties. *Adv. Heat Transf.* **6**, 503–564.
- PINELLI, A., UHLMANN, M., SEKIMOTO, A. & KAWAHARA, G. 2010 Reynolds number dependence of mean flow structure in square duct turbulence. *J. Fluid Mech.* **644**, 107–122.
- PIROZZOLI, S. 2014 Revisiting the mixing-length hypothesis in the outer part of turbulent wall layers: mean flow and wall friction. *J. Fluid Mech.* **745**, 378–397.
- PIROZZOLI, S. 2023 An explicit representation for mean profiles and fluxes in forced passive scalar convection. *J. Fluid Mech.* **968**, R1.
- PIROZZOLI, S., BERNARDINI, M. & ORLANDI, P. 2016 Passive scalars in turbulent channel flow at high Reynolds number. *J. Fluid Mech.* **788**, 614–639.
- PIROZZOLI, S., BERNARDINI, M., VERZICCO, R. & ORLANDI, P. 2017 Mixed convection in turbulent channels with unstable stratification. *J. Fluid Mech.* **821**, 482–516.
- PIROZZOLI, S. & MODESTI, D. 2023 Direct numerical simulation of one-sided forced thermal convection in plane channels. *J. Fluid Mech.* **957**, A31.
- PIROZZOLI, S. & MODESTI, D. 2024 Mean temperature and concentration profiles in turbulent internal flows. *Int. J. Heat Fluid Flow (Under review)*, <https://arxiv.org/abs/2403.17689>.
- SIEDER, E.N. & TATE, G.E. 1936 Heat transfer and pressure drop of liquids in tubes. *Ind. Eng. Chem.* **28** (12), 1429–1435.
- SLEICHER, C.A. & ROUSE, M.W. 1975 A convenient correlation for heat transfer to constant and variable property fluids in turbulent pipe flow. *Int. J. Heat Mass Transf.* **18** (5), 677–683.
- SPARROW, E.M., LLOYD, J.R. & HIXON, C.W. 1966 Experiments on turbulent heat transfer in an asymmetrically heated rectangular duct. *J. Heat. Transfer* pp. 170–174.
- TRETTEL, A. & LARSSON, J. 2016 Mean velocity scaling for compressible wall turbulence with heat transfer. *Phys. Fluids (1994-present)* **28** (2), 026102.
- WHITE, F. M. 1974 *Viscous fluid flow*. McGraw-Hill, New York.
- XIA, Y., ROWIN, W.A., JELLY, T., MARUSIC, I. & HUTCHINS, N. 2022 Investigation of cold-wire spatial and temporal resolution issues in thermal turbulent boundary layers. *Int. J. Heat Fluid Flow* **94**, 108926.
- YEH, F.C. & STEPKA, F.S. 1984 Review and status of heat-transfer technology for internal passages of air-cooled turbine blades. NASA Technical Paper 2232. NASA.
- YERRAGOLAM, G.S., HOWLAND, C.J., STEVENS, R.J.A.M., VERZICCO, R., SHISHKINA, O. & LOHSE, D. 2024 Scaling relations for heat and momentum transport in sheared Rayleigh–Bénard convection. *arXiv preprint arXiv:2403.04418*.

- ZHONG, K., HUTCHINS, N. & CHUNG, D. 2023 Heat-transfer scaling at moderate prandtl numbers in the fully rough regime. *J. Fluid Mech.* **959**, A8.
- ZONTA, F. 2013 Nusselt number and friction factor in thermally stratified turbulent channel flow under non-Oberbeck–Boussinesq conditions. *Int. J. Heat Fluid Flow* **44**, 489–494.
- ZONTA, F., MARCHIOLI, C. & SOLDATI, A. 2012 Modulation of turbulence in forced convection by temperature-dependent viscosity. *J. Fluid Mech.* **697**, 150–174.